Science Advances
AAAS

Supplementary Materials for

Synthetic enforcement of STING signaling in cancer cells appropriates the immune microenvironment for checkpoint inhibitor therapy

Larsen Vornholz *et al.*

Corresponding author: Jürgen Ruland, j.ruland@tum.de

Sci. Adv. **9**, eadd8564 (2023)
DOI: 10.1126/sciadv.add8564

The PDF file includes:

Figs. S1 to S7
Legends for tables S1 to S3

Other Supplementary Material for this manuscript includes the following:

Tables S1 to S3

SUPPLEMENTARY FIGURES

Fig. S1. GSEA of dMMR vs. pMMR human primary organoids.

(A) GSEA of differentially expressed gene sets from the Reactome database comparing pMMR vs. dMMR tumor organoids (+ve NES: dMMR).

Fig. S2. cGAS/STING controls IFN signaling in dMMR tumor cells.

(A, B) Genetically modified MC38 tumor cells were confirmed by western blotting. (C) Cytosolic DNA of MC38 tumor cells was isolated with a commercial kit and quantified by qPCR with primers specific for genomic DNA. (D) Cytosolic cGAMP levels were quantified by ELISA of cell lysates of cultured MC38 tumor cells. (E) IFN-β production from MC38 tumor cells was quantified by ELISA. (F) Cytosolic DNA of MC38 tumor cells was isolated with a commercial kit and quantified by qPCR with primers specific for genomic DNA. (G) Cytosolic cGAMP levels were quantified by ELISA of cell lysates of cultured MC38 tumor cells. (H) IFN-β production from MC38 tumor cells was quantified by ELISA. (I) The phosphorylation of STAT1 in cultured MC38 cells was detected by western blotting. (J) The relative gene expression of *Isg15, Ccl5* and *Cxcl10* in cultured MC38 tumor cells was quantified by qPCR. (K) The phosphorylation of STAT1 in cultured MC38 cells was detected by western blotting. (L) The relative gene expression of *Isg15, Ccl5* and *Cxcl10* in cultured MC38 tumor cells was quantified by qPCR. The data represent n=3 independent experiments (C, D, F, G, J, L) or are representative of n=2 independent experiments (E, H). One-way ANOVA (D, E, G, H, J, L) or Student's t test (C, F) was used to determine significance.

Fig. S3. STING-mediated IFN signaling in dMMR CRC controls immunogenicity.

(A, B) Genetically modified MC38 tumor cells were treated with anti-IFNAR1 blocking antibodies (30 μg/ml) for 24 h, and the relative gene expression of *Isg15*, *Ccl5* and *Cxcl10* was quantified by qPCR. (C, D) *In vitro* proliferation of cultured MC38 tumor cells. (E) Endpoint size of subcutaneously grown WT, MLH1-/- or MLH1/STING-/- MC38 tumors (n=5) or (F) WT, MSH2-/- or MSH2/STING-/- MC38 tumors (n=7-10). (G, H) Tumor-bearing mice were treated without or with anti-IFNAR1 (200 μg/mouse) blocking antibodies every three days starting at Day 0 (n=3-5). (I, J) Tumor-bearing mice were treated without or with anti-CXCR3 (200 μg/mouse) blocking antibodies every three days starting at Day 0 (n=3-5). The data are representative of n=2 independent experiments (A, B) or represent n=3 independent experiments (C, D). The data are presented as the mean ± SEM (G-J). One-way ANOVA (E, F) or Student's t test (A, B) was used to determine significance.

Fig. S4. Synthetically enforced STING^{N153S} drives IFN signaling.

(A) IFN-β production from STING mutant MC38 tumor cells was quantified by ELISA. (B) The phosphorylation of STAT1 in cultured STING mutant MC38 cells was detected by western blotting. (C) The relative gene expression of *Isg15* in cultured STING mutant MC38 tumor cells was quantified by qPCR. The data are representative of n=2 independent experiments (A, C). One-way ANOVA (A, C) was used to determine significance.

Fig. S5. Synthetically enforced STING signaling promotes antitumor immunity.

(A) Endpoint tumor weight of subcutaneously grown WT vs. STING^{N153S} MC38 tumors in syngeneic WT C57Bl/6 mice (n=5). (B) *In vitro* proliferation of cultured MC38 tumor cells. (C) Growth of subcutaneously inoculated WT and STING^{N153S} MC38 tumor cells in NOD-SCID mice (n=4). (D) *In vitro* proliferation of cultured STING mutant MC38 tumor cells. (E) Growth of subcutaneously inoculated STING mutant MC38 tumor cells in syngeneic C57Bl/6

mice (n=5). (F) FACS analyses displaying the percentages of Ifng and PD1 in CD8+ T cells from subcutaneously grown MC38 tumors in syngeneic WT C57Bl/6 mice explanted on Day 16. The data are presented as the mean ± SEM from n=3 independent experiments (B) or are representative of n=2 independent experiments (D). Student´s t test (A, F) was used to determine significance.

Fig. S6. Tumor cell-intrinsic STING enforcement sensitizes to immune checkpoint inhibitor therapy.

(A) Endpoint tumor weight of subcutaneously grown WT vs. mixSTING^{N153S} MC38 tumors that were treated with ICI therapy (n=10). (B) Survival of WT vs. mixSTING^{N153S} tumor-bearing mice treated with ICI therapy every three days starting on Day 10 (n=9-10). Student´s t test (A) or log-rank (Mantel–Cox) test (B) was used to determine significance.

Fig. S7. The expression of STING^{N153S} in a subset of tumor cells reprograms the TME.

(A) Heatmap displaying the different cell clusters (y-axis) and the antigen intensity of the antibody-labeled cells (x-axis). (B) UMAP plot displaying the annotated clusters comparing the WT (gray) vs. mixSTING^{N153S} (blue) conditions. (C) WT or mixSTING^{N153S} MC38 tumor cells were subcutaneously inoculated into syngeneic C57Bl/6 mice, and the percentages (CD4, CD8, NK, CD11c, CD8+ DCs) of live/CD45+ cells in the tumor were quantified by FACS analysis (n=4-5). (D) Differentially expressed gene sets obtained via GSEA by using g:profiler on all GO:BP terms enriched for fewer than 400 genes considering only the DC clusters “MHCII+ DCs” and “CD11b+ DCs”. Student´s t test (C) was used to determine significance.

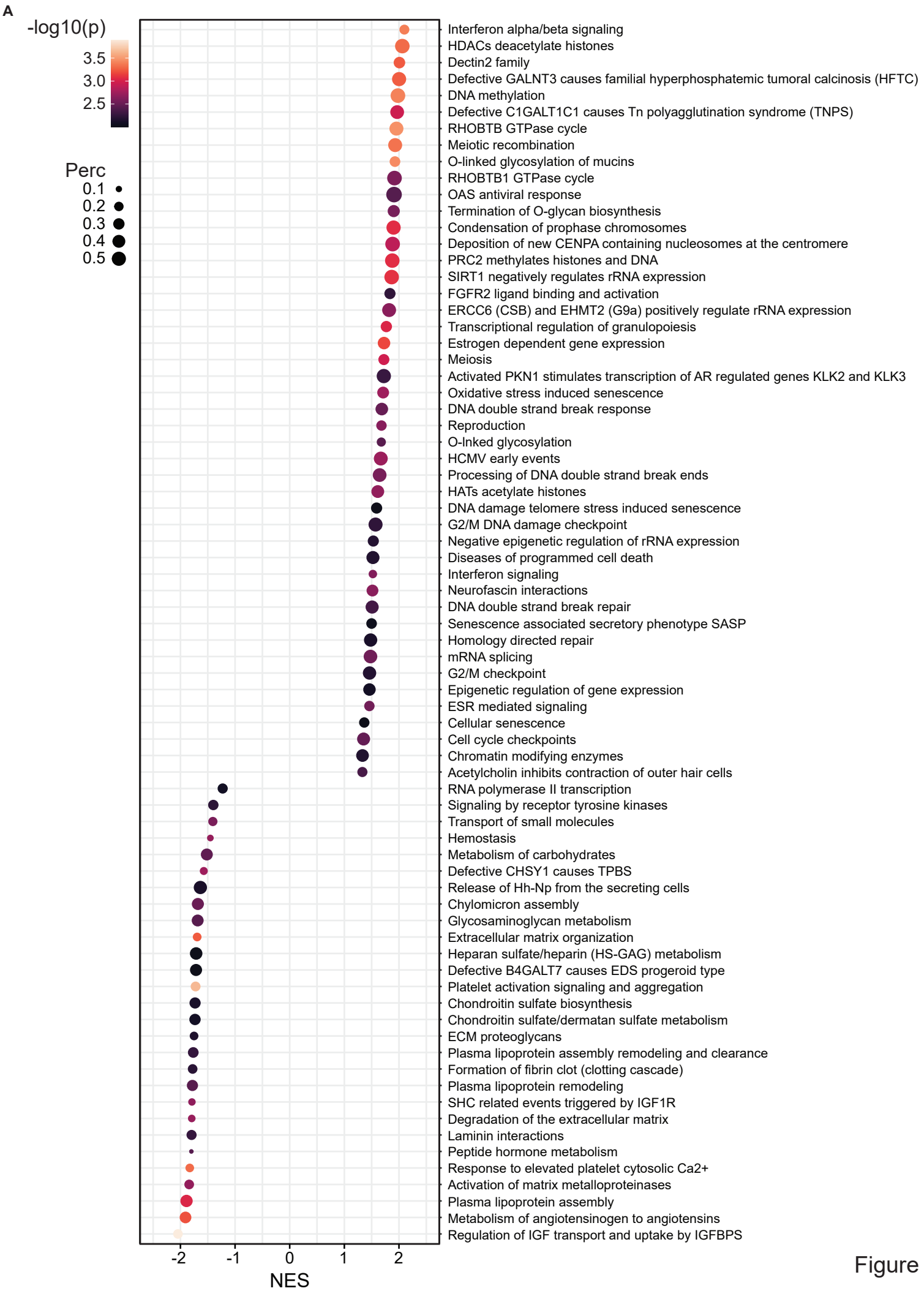
A
-log10(p)
3.5
3.0
2.5
Perc
0.1
0.2
0.3
0.4
0.5
Interferon alpha/beta signaling
HDACs deacetylate histones
Dectin2 family
Defective GALNT3 causes familial hyperphosphatemic tumoral calcinosis (HFTC)
DNA methylation
Defective C1GALT1C1 causes Tn polyagglutination syndrome (TNPS)
RHOBTB GTPase cycle
Meiotic recombination
O-linked glycosylation of mucins
RHOBTB1 GTPase cycle
OAS antiviral response
Termination of O-glycan biosynthesis
Condensation of prophase chromosomes
Deposition of new CENPA containing nucleosomes at the centromere
PRC2 methylates histones and DNA
SIRT1 negatively regulates rRNA expression
FGFR2 ligand binding and activation
ERCC6 (CSB) and EHMT2 (G9a) positively regulate rRNA expression
Transcriptional regulation of granulopoiesis
Estrogen dependent gene expression
Meiosis
Activated PKN1 stimulates transcription of AR regulated genes KLK2 and KLK3
Oxidative stress induced senescence
DNA double strand break response
Reproduction
O-lnked glycosylation
HCMV early events
Processing of DNA double strand break ends
HATs acetylate histones
DNA damage telomere stress induced senescence
G2/M DNA damage checkpoint
Negative epigenetic regulation of rRNA expression
Diseases of programmed cell death
Interferon signaling
Neurofascin interactions
DNA double strand break repair
Senescence associated secretory phenotype SASP
Homology directed repair
mRNA splicing
G2/M checkpoint
Epigenetic regulation of gene expression
ESR mediated signaling
Cellular senescence
Cell cycle checkpoints
Chromatin modifying enzymes
Acetylcholin inhibits contraction of outer hair cells
RNA polymerase II transcription
Signaling by receptor tyrosine kinases
Transport of small molecules
Hemostasis
Metabolism of carbohydrates
Defective CHSY1 causes TPBS
Release of Hh-Np from the secreting cells
Chylomicron assembly
Glycosaminoglycan metabolism
Extracellular matrix organization
Heparan sulfate/heparin (HS-GAG) metabolism
Defective B4GALT7 causes EDS progeroid type
Platelet activation signaling and aggregation
Chondroitin sulfate biosynthesis
Chondroitin sulfate/dermatan sulfate metabolism
ECM proteoglycans
Plasma lipoprotein assembly remodeling and clearance
Formation of fibrin clot (clotting cascade)
Plasma lipoprotein remodeling
SHC related events triggered by IGF1R
Degradation of the extracellular matrix
Laminin interactions
Peptide hormone metabolism
Response to elevated platelet cytosolic Ca2+
Activation of matrix metalloproteinases
Plasma lipoprotein assembly
Metabolism of angiotensinogen to angiotensins
Regulation of IGF transport and uptake by IGFBPS
-2
-1
0
1
2
NES

Figure S1

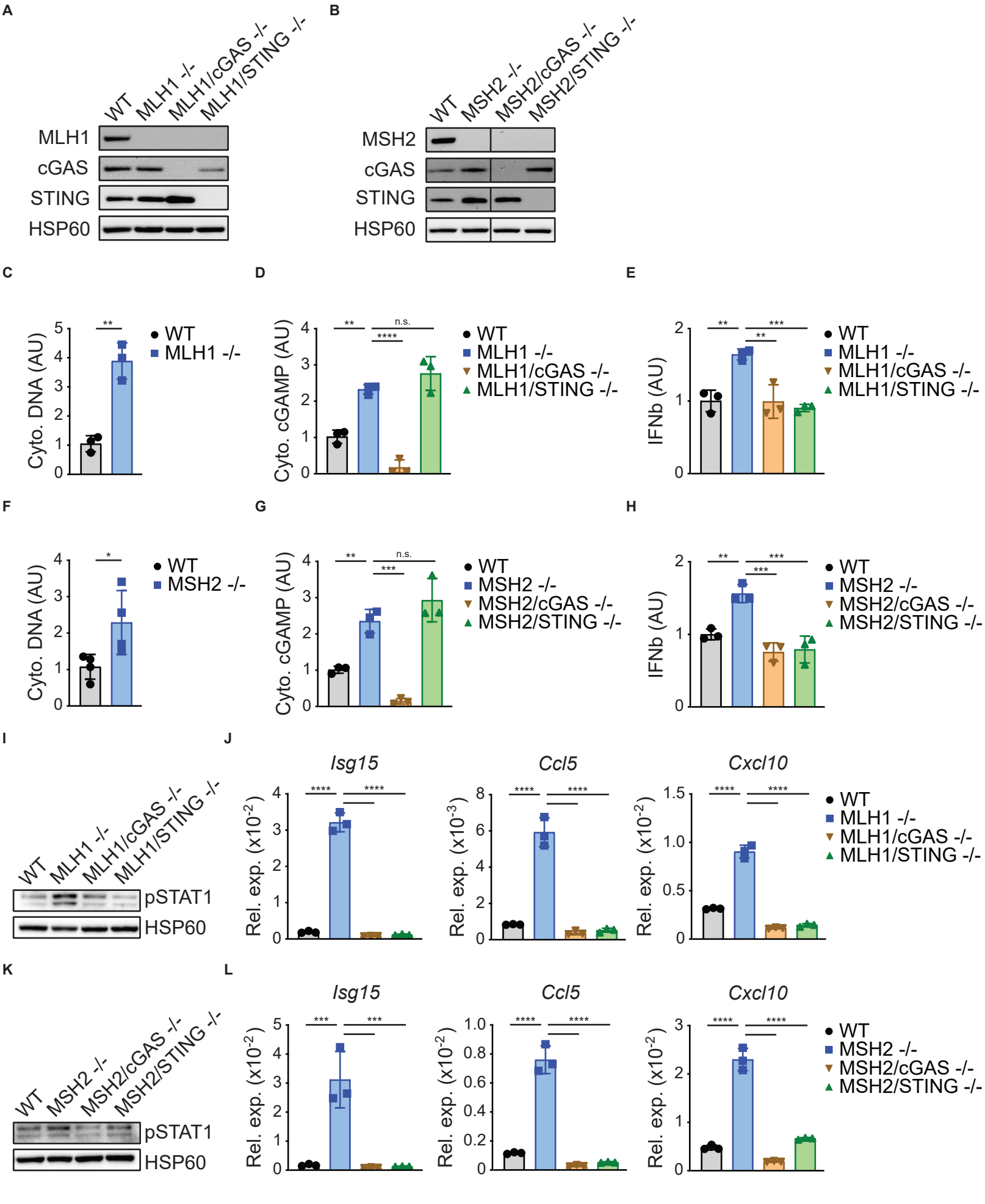
A
WT
MLH1 -/-
MLH1/cGAS -/-
MLH1/STING -/-
MLH1
cGAS
STING
HSP60
B
WT
MSH2 -/-
MSH2/cGAS -/-
MSH2/STING -/-
MSH2
cGAS
STING
HSP60
C
Cyto. DNA (AU)
WT
MLH1 -/-
D
Cyto. cGAMP (AU)
n.s.
WT
MLH1 -/-
MLH1/cGAS -/-
MLH1/STING -/-
E
IFNb (AU)
F
Cyto. DNA (AU)
WT
MSH2 -/-
G
Cyto. cGAMP (AU)
n.s.
WT
MSH2 -/-
MSH2/cGAS -/-
MSH2/STING -/-
H
IFNb (AU)
I
WT
MLH1 -/-
MLH1/cGAS -/-
MLH1/STING -/-
pSTAT1
HSP60
J
Isg15
Ccl5
Cxcl10
Rel. exp. (x10-2)
Rel. exp. (x10-3)
WT
MLH1 -/-
MLH1/cGAS -/-
MLH1/STING -/-
K
WT
MSH2 -/-
MSH2/cGAS -/-
MSH2/STING -/-
pSTAT1
HSP60
L
Isg15
Ccl5
Cxcl10
Rel. exp. (x10-2)
WT
MSH2 -/-
MSH2/cGAS -/-
MSH2/STING -/-

Figure S2

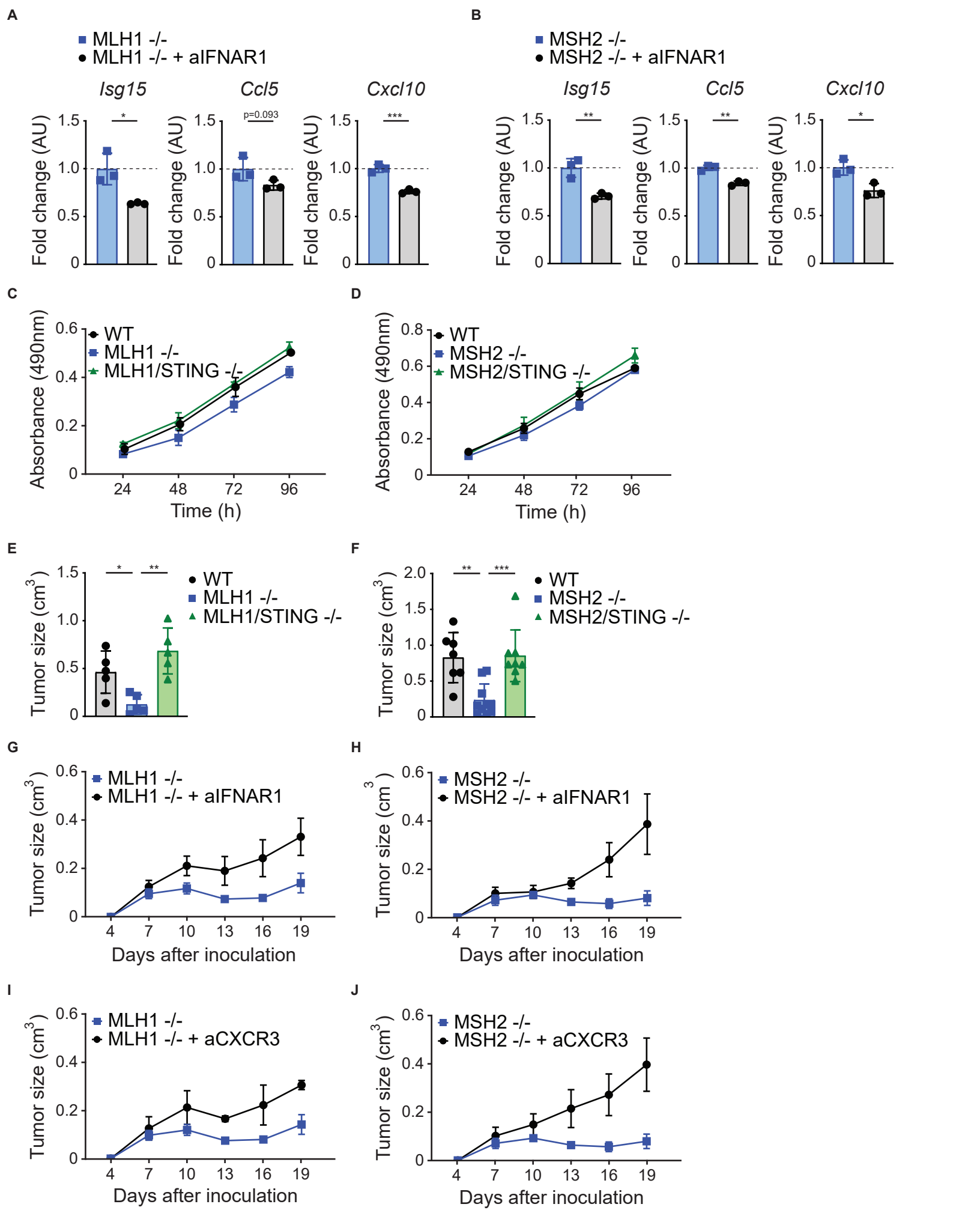
A
MLH1 -/-
MLH1 -/- + aIFNAR1
Isg15
Ccl5
Cxcl10
Fold change (AU)
p=0.093
B
MSH2 -/-
MSH2 -/- + aIFNAR1
C
WT
MLH1 -/-
MLH1/STING -/-
Absorbance (490nm)
Time (h)
D
MSH2 -/-
MSH2/STING -/-
E
Tumor size (cm3)
F
G
Days after inoculation
H
I
MLH1 -/- + aCXCR3
J
MSH2 -/- + aCXCR3

Figure S3

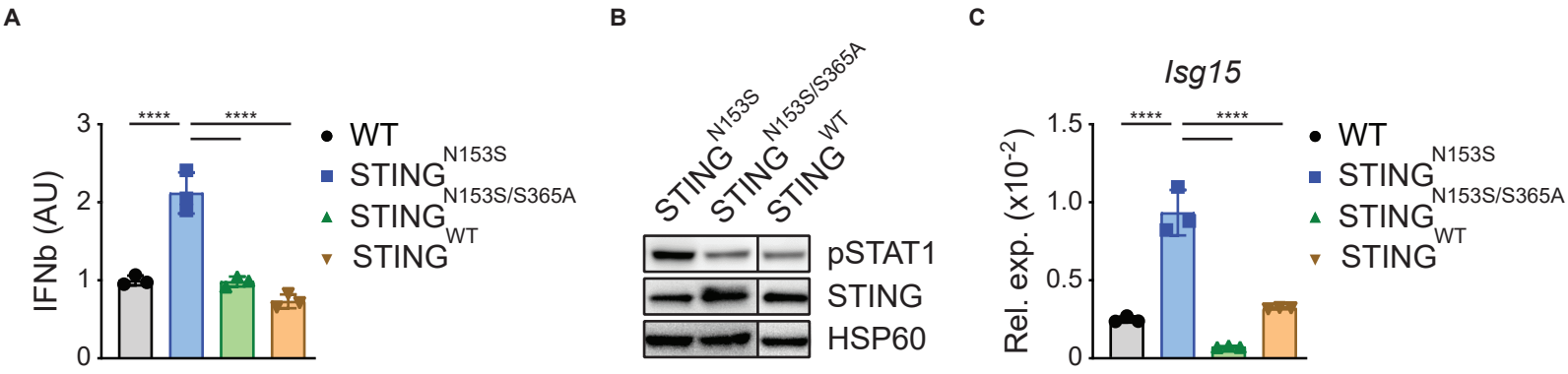
A
IFNb (AU)
3
2
1
0
****
****
WT
STING N153S
STING N153S/S365A
STING WT
B
STING N153S
STING N153S/S365A
STING WT
pSTAT1
STING
HSP60
C
Isg15
Rel. exp. (x10-2)
1.5
1.0
0.5
0
****
****
WT
STING N153S
STING N153S/S365A
STING WT

Figure S4

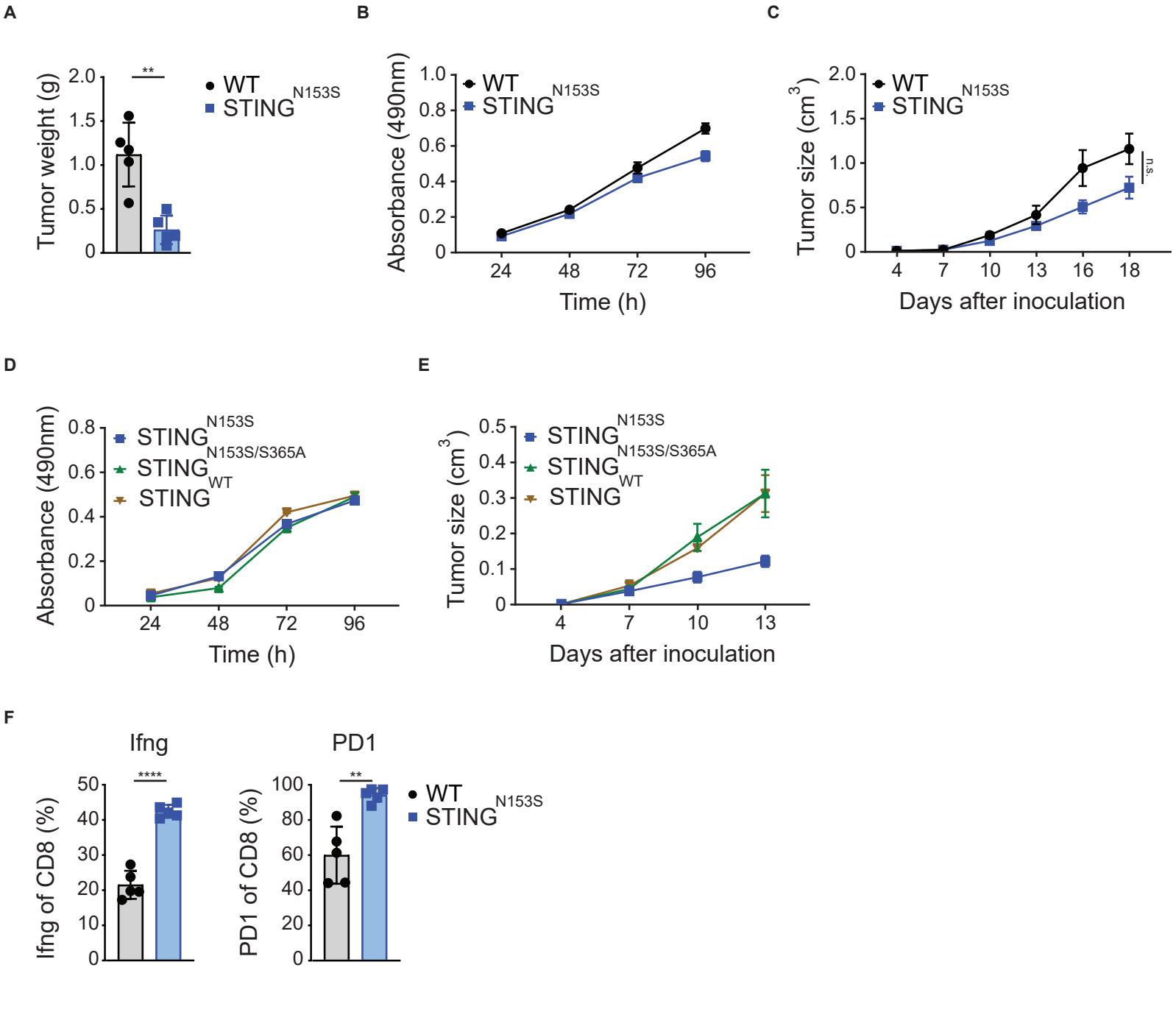
A
Tumor weight (g)
2.0
1.5
1.0
0.5
0
**
WT
STING N153S
B
Absorbance (490nm)
1.0
0.8
0.6
0.4
0.2
0
WT
STING N153S
24
48
72
96
Time (h)
C
Tumor size (cm 3)
2.0
1.5
1.0
0.5
0
WT
STING N153S
n.s.
4
7
10
13
16
18
Days after inoculation
D
Absorbance (490nm)
0.8
0.6
0.4
0.2
0
STING N153S
STING N153S/S365A
STING WT
24
48
72
96
Time (h)
E
Tumor size (cm 3)
0.5
0.4
0.3
0.2
0.1
0
STING N153S
STING N153S/S365A
STING WT
4
7
10
13
Days after inoculation
F
Ifng
Ifng of CD8 (%)
50
40
30
20
10
0
****
PD1
PD1 of CD8 (%)
100
80
60
40
20
0
**
WT
STING N153S

Figure S5

A

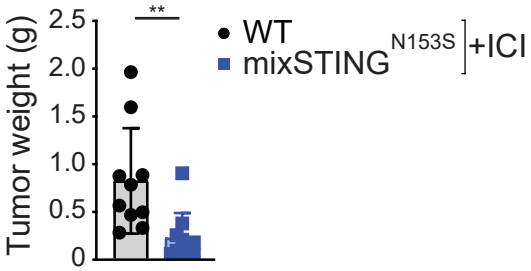
Tumor weight (g)
2.5
2.0
1.5
1.0
0.5
0
**
WT
mixSTING N153S
+ICI

B

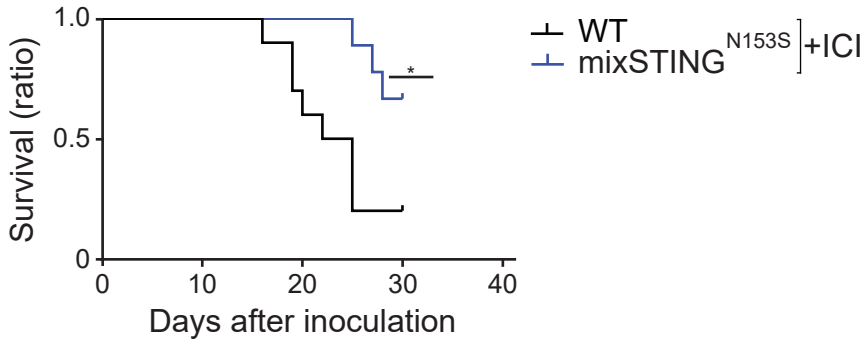
Survival (ratio)
1.0
0.5
0
0
10
20
30
40
Days after inoculation
*
WT
mixSTING N153S
+ICI

Figure S6

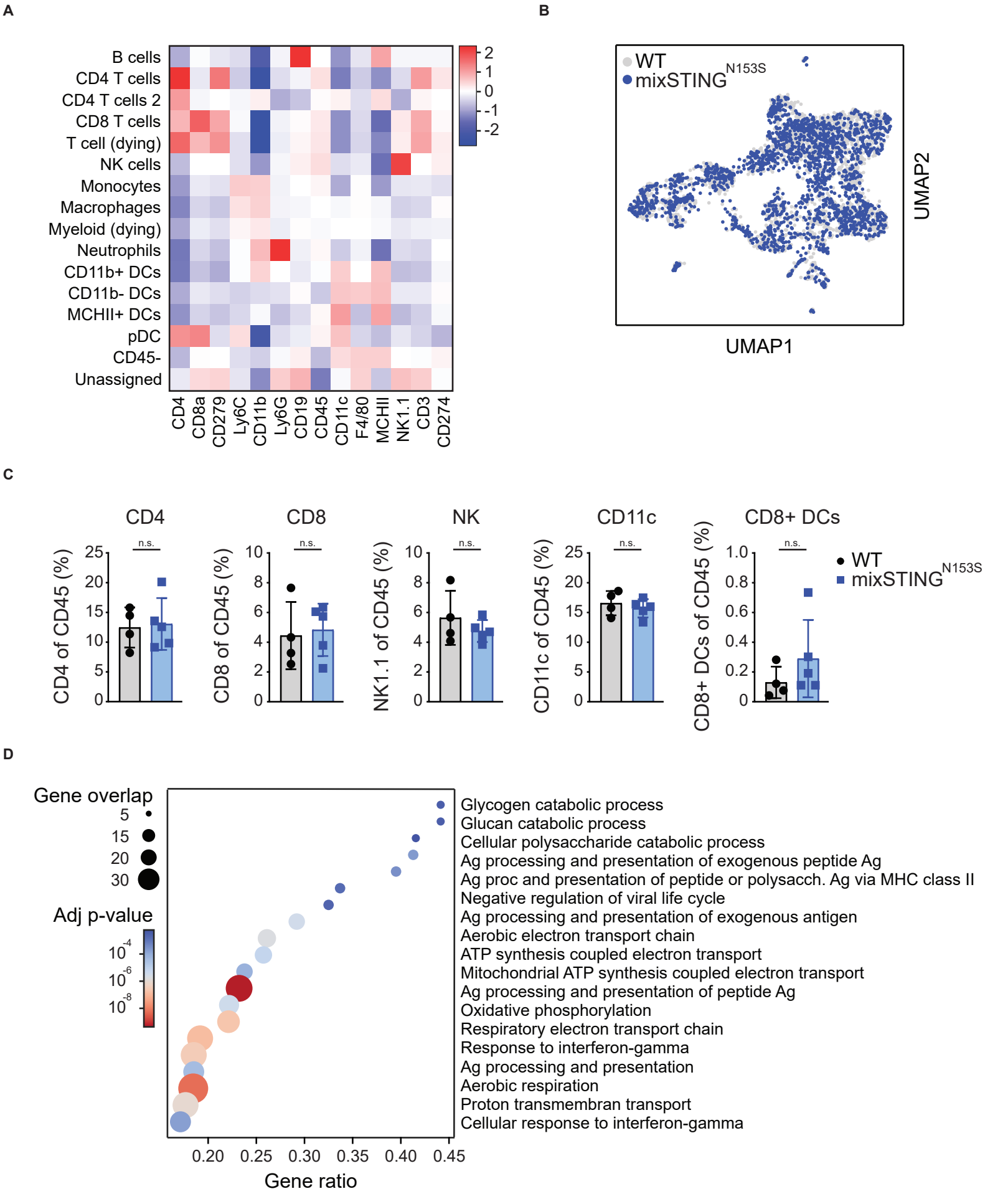
A
B cells
CD4 T cells
CD4 T cells 2
CD8 T cells
T cell (dying)
NK cells
Monocytes
Macrophages
Myeloid (dying)
Neutrophils
CD11b+ DCs
CD11b- DCs
MCHII+ DCs
pDC
CD45-
Unassigned
CD4
CD8a
CD279
Ly6C
CD11b
Ly6G
CD19
CD45
CD11c
F4/80
MCHII
NK1.1
CD3
CD274
2
1
0
-1
-2
B
WT
mixSTING N153S
UMAP2
UMAP1
C
CD4
CD8
NK
CD11c
CD8+ DCs
CD4 of CD45 (%)
CD8 of CD45 (%)
NK1.1 of CD45 (%)
CD11c of CD45 (%)
CD8+ DCs of CD45 (%)
n.s.
WT
mixSTING N153S
D
Gene overlap
5
15
20
30
Adj p-value
10-4
10-6
10-8
0.20
0.25
0.30
0.35
0.40
0.45
Gene ratio
Glycogen catabolic process
Glucan catabolic process
Cellular polysaccharide catabolic process
Ag processing and presentation of exogenous peptide Ag
Ag proc and presentation of peptide or polysacch. Ag via MHC class II
Negative regulation of viral life cycle
Ag processing and presentation of exogenous antigen
Aerobic electron transport chain
ATP synthesis coupled electron transport
Mitochondrial ATP synthesis coupled electron transport
Ag processing and presentation of peptide Ag
Oxidative phosphorylation
Respiratory electron transport chain
Response to interferon-gamma
Ag processing and presentation
Aerobic respiration
Proton transmembran transport
Cellular response to interferon-gamma

Figure S7

Table S1. Mutations in MMR genes in human CRC from TCGA datasets and in patient-derived CRC organoids.

Table S2. Total number of somatic variants and variant allele frequencies of recurrent mutations in dMMR (n=3) and pMMR (n=9) patient-derived CRC organoids.

Table S3. Differential gene expression analysis (DESeq2 output and GSEA) comparing human dMMR (n=3) vs. pMMR (n=9) patient-derived CRC organoids.